Radical Pair and Triplet State Dynamics of a Photosynthetic Reaction-Center Model Embedded in Isotropic Media and Liquid Crystals

Kobi Hasharoni,[†] Haim Levanon,*[,†] Scott R. Greenfield,[‡] David, J. Gosztola,[‡] Walter A. Svec,[‡] and Michael R. Wasielewski*[,‡,§]

Contribution from the Department of Physical Chemistry and The Farkas Center for Light-Induced Processes, The Hebrew University of Jerusalem, Jerusalem 91904, Israel, Chemistry Division, Argonne National Laboratory, Argonne, Illinois, 60439, and Department of Chemistry, Northwestern University, Evanston, Illinois 60208

Received June 7, 1996[⊗]

Abstract: The electron spin dynamics associated with intramolecular electron transfer in a photosynthetic model system, which consists of a linear structure of the type A-B-C, is described. In this structure, donor A is a *p*-methoxyaniline, chromophore B is a 4-amino-1,8-naphthalimide, and acceptor C is a 1,4:5,8-naphthalenediimide. This supramolecular electron donor−acceptor array was isotropically oriented in toluene, and anisotropically oriented in liquid crystal matrices, and studied by time-resolved electron paramagnetic resonance spectroscopy. Photoexcitation of B results in a two-step electron transfer to yield the radical ion pair, $A^{\bullet+}$-B-$C^{\bullet-}$. Charge recombination within $A^{\bullet+}$-B-$C^{\bullet-}$ produces a molecular triplet state, A-B-^{3*}C, which exhibits the unique spin-polarized electron paramagnetic resonance signal that has been observed only in photosynthetic reaction-center proteins.

Introduction

Intramolecular electron transfer (IET) is the subject of many studies that are aimed at elucidating the role of the various parameters which govern the IET rate.[1] One of the major goals of such studies is the successful mimicry of the efficient charge separation that occurs in the photosynthetic reaction center. This goal can be achieved by using synthetic models that optimize the relative orientations, distances, and electronic couplings between the participating redox partners. The chromophores used in such models may be either the ones that are found in the natural system, e.g., chlorophylls, pheophytins, and quinones, or specific molecules not found in nature, that are known to be efficient electron donors and acceptors.

In a recent communication, we have described the IET process found in a linear model system with an A-B-C structure, **1**.[2] In this structure, the donor A is a *p*-methoxyaniline, B is a 4-amino-1,8-naphthalimide, and acceptor C is a 1,4:5,8-naphthalenediimide. The design of supermolecule **1** follows criteria established for promoting high quantum yield charge separation in glassy media.[3a] The lowest excited singlet state of chromophore B is a charge transfer state that is easily oxidized or reduced.[3b] Donor A and acceptor C were chosen primarily for their redox properties and the distinct optical spectra that result when donor A is oxidized[3c] and acceptor C is reduced.[3d] By employing time-resolved electron paramagnetic resonance (TREPR) and fast transient optical absorption spectroscopies, we have demonstrated that a two-step IET occurs upon photoexcitation of B, which yields the radical ion pair, $A^{\bullet+}$-B-$C^{\bullet-}$. Charge recombination within this radical pair (RP) produces a molecular triplet state, A-B-^{3*}C, whose unique EPR features are similar to those observed only in bacterial[4] and in green plant photosystems I[5] and II.[6]

This paper quantifies the preliminary results reported recently. We present here a complete description of the excited state reactions and line shape analyses attributed to the paramagnetic states involved, i.e., the triplet and radical pair. Molecular modeling[7] of **1** shows that the molecule is cylindrical except for the aliphatic chain connected to the C fragment, which is tilted away from the cylindrical axis of the molecule. The A-to-C and B-to-C center-to-center distances are ∼24 and ∼18 Å, respectively. A-B-C and its separate fragments (**1**, **2**, **4**, and **5**, respectively) were studied in both conventional isotropic solvents and anisotropic liquid crystals (LC).

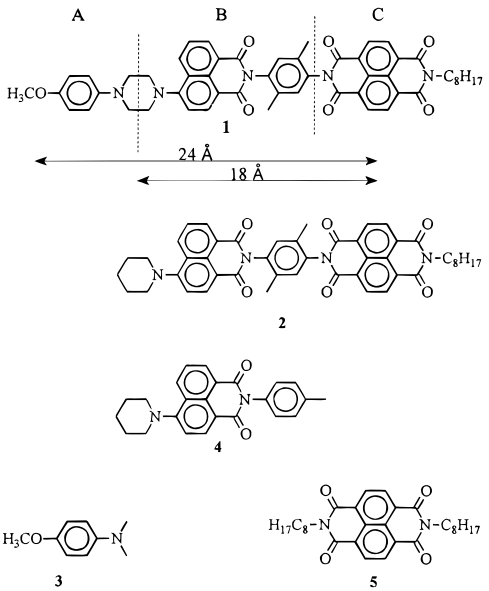

[†] The Hebrew University of Jerusalem.
[‡] Argonne National Laboratory.
[§] Northwestern University.
[⊗] Abstract published in *Advance ACS Abstracts,* October 1, 1996.

(1) (a) Joran, A. D.; Leland, B. A.; Felker, P. M.; Zewail, A. H.; Hopfield, J. J.; Dervan, P. B. *Nature* **1987**, *327*, 508. (b) Wasielewski, M. R. *Chem. Rev.* **1992**, *92*, 435. (c) Gust, D.; Moore, T. A.; Moore, A. L. *Acc. Chem. Res.* **1993**, *26*, 198.

(2) Hasharoni, K.; Levanon, H.; Greenfield, S. R.; Gosztola, D. J.; Svec, W. A.; Wasielewski, M. R. *J. Am. Chem. Soc.* **1995**, *117*, 8055.

(3) (a) Gaines, G. L.; O'Neil, M. P.; Svec, W. A.; Niemczyk, M. P.; Wasielewski, M. R. *J. Am. Chem. Soc.* **1991**, *113*, 719. (b) Alexiou, M. S.; Tychopoulos, V.; Ghorbanian, S.; Tyman, J. H. P.; Brown, R. G.; Brittain, P. I. *J. Chem. Soc., Perkin Trans. 2* **1990**, 837. (c) Hester, R. A.; Williams, K. P. J. *J. Chem. Soc., Perkin Trans. 2* **1982**, 559. (d) Viehbeck, A.; Goldberg, M. J.; Kovac, C. A. *J. Electrochem. Soc.* **1990**, *137*, 1460.

S0002-7863(96)01919-1 CCC: $12.00

As was demonstrated previously, LCs are suitable matrices for TREPR studies in the fluid phase for both triplet[8] and IET[9] studies. The advantages of using LCs are 2-fold. First, the anisotropy imposed by the LC on the guest chromophore is significant in the interpretation of orientational effects on the spectrum. The second is due to the anisotropic dielectric properties of LCs, which slow down the IET rate into the TREPR time scale, thus enabling the utilization of EPR spectroscopy with its high spectral resolution to study the products of ultrafast charge separation processes.

Experimental Section

Molecules **1**−**5** were prepared as described elsewhere.[10] Toluene (Merck Ltd.) was dried over a Na/K mirror overnight and was kept under vacuum throughout sample preparation. Two LCs (Merck Ltd.) with different dielectric constants (E-7: $\epsilon = 19.0$, ZLI-4389: $\epsilon = 56.0$)[11] were used and are characterized by the following phase transition temperatures:[12]

E-7: crystalline $\overset{210\ K}{\longleftrightarrow}$ soft cryst. $\overset{263\ K}{\longleftrightarrow}$ nematic $\overset{333\ K}{\longleftrightarrow}$ isotropic

ZLI-4389:

crystalline $\overset{250\ K}{\longleftrightarrow}$ soft cryst. $\overset{253\ K}{\longleftrightarrow}$ nematic $\overset{335\ K}{\longleftrightarrow}$ isotropic

toluene: crystalline $\overset{\sim 160\ K}{\longleftrightarrow}$ soft cryst. $\overset{177\ K}{\longleftrightarrow}$ isotropic (1)

Samples of **1**, **2**, **4**, **5** were first dissolved in toluene (∼1 mM), which was then evaporated, and the LC was introduced into 4 mm o.d. Pyrex tubes and degassed by several freeze-pump-thaw cycles on a vacuum line. The temperature was maintained using a nitrogen variable-temperature flow dewar in the EPR resonator. The samples were excited at 420 nm by a dye laser (Quanta Ray, DCR-1A, 1 mJ/pulse at a repetition rate of 10 Hz) pumped by the third harmonic of a Nd:YAG laser (Quanta Ray PDL-1), which excites exclusively the B moiety in **1** and **2**. CW-TREPR measurements were carried out on a Bruker ESP-380 spectrometer with the field modulation disconnected as described elsewhere.[9]

The orientation of the LC director, **L**, with respect to the magnetic field, **B**, is determined by the sign of the diamagnetic susceptibility ($\chi_{\parallel} - \chi_{\perp} = \Delta\chi$). In all LCs used here, $\Delta\chi$ is positive and as a consequence, the default orientation is **L** || **B**.

Results

Triplet Line Shape Analysis. The EPR line shape analysis of triplet states using the density matrix formalism has been described elsewhere.[13,14] The imaginary part of the magnetic susceptibility, χ'', in anisotropic matrices with cylindrical distribution of the chromophores about **L** is given by

$$\chi''(\mathbf{B},t) \propto \sum_{\substack{i=1,2 \\ j=i+1}} \int_0^{\pi/2} f(\theta') \int_{\theta_{min}}^{\pi/2} \int_0^{\pi/2} Im[\rho_{ij}(\theta,\phi,t)] f(\phi) d\theta d\phi d\theta' \quad (2)$$

where θ and ϕ define the relation between **B** and the molecular axes, and $\rho_{i,j}(\theta,\phi,t)$ is the density matrix element connecting the i,j levels. The summation is made over the two possible transitions, and, because of symmetry, the integration is carried out over one octant of space. The fluctuations of the molecular plane about **L** are expressed by $f(\theta') = \cos^2(\theta') \exp(-\theta'^2/\sigma_{\theta}^2)$, and $\theta_{min} = (\pi/2) - \alpha \pm \theta'$ where α is the sample rotation angle about an axis perpendicular to **B**. The sign of θ' is chosen such that $0 \le \theta_{min} \le \pi/2$. The preferred orientation of the guest chromophore in the LC is given by the angle ϕ_0, and its fluctuations are described by $f(\phi)$ which is a Gaussian with variance σ_{ϕ}^2. In order to improve the accuracy of these multiparameter simulations, variation of the parameters was carried out by using the downhill simplex algorithm,[15] until the residuals between the spectrum and fit reached a minimum.

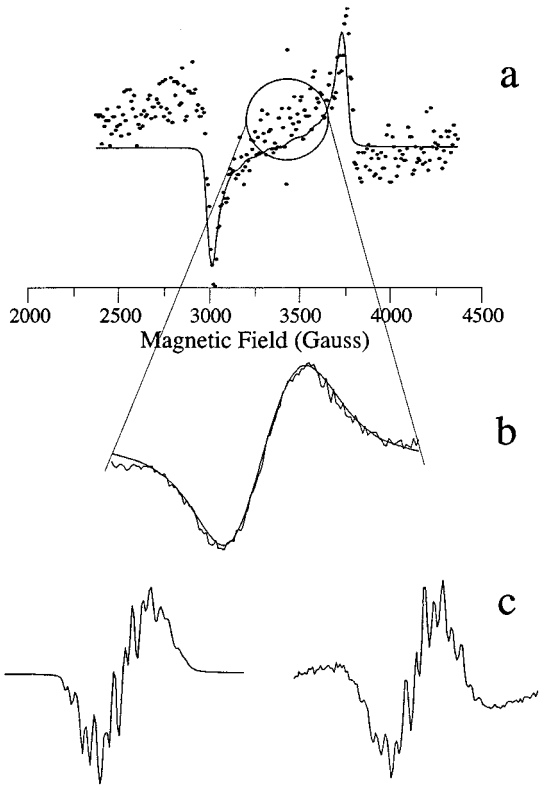

Figure 1. TREPR spectra of **1** in toluene at 5 mW mw power: (a) A-B-^{3*}C at 150 K, 700 ns following the laser pulse (420 nm). (b) A$^{\bullet+}$-B-C$^{\bullet-}$ at 150 K, 1000 ns following the laser pulse. (c) Right: A$^{\bullet+}$-B-C$^{\bullet-}$ at 210 K, 1000 ns following the laser pulse, left: line shape simulation. The scan range of the expanded spectra is 25 G. The smooth curves superimposed on the spectra are simulation of eq 2 (a) and eqs 5−9 (b and c) with parameters given in Table 1.

A-B-C (1) in Toluene. The EPR spectra in Figure 1 exhibit two major features: a broad triplet spectrum with a width of ∼750 G, exhibiting an *e,a* (emission/absorption) phase pattern

(4) Dutton, P. L.; Leigh, J. S.; Seibert, M. *Biochem. Biophys. Res. Commun.* **1972**, *46*, 406.

(5) Regev, A.; Nechushtai, R.; Levanon, H.; Thornber, J. P. *J. Phys. Chem.* **1989**, *93*, 2421.

(6) Rutherford, A. W.; Paterson, D. R.; Mullet, J. E. *Biochim. Biophys. Acta* **1981**, *635*, 205.

(7) The minimum-energy geometry of ABC was determined from an INDO calculation with HyperChem (Hypercube Inc.).

(8) Regev, A.; Levanon, H.; Murai, T.; Sessler, J. L. *J. Chem. Phys.* **1990**, *92*, 4718.

(9) (a) Hasharoni, K.; Levanon, H.; von Gersdorff, J.; Kurreck, H.; Möbius, K. *J. Chem. Phys.* **1993**, *98*, 2916. (b) Hasharoni, K.; Levanon, H.; Gätschmann, J.; Schubert, H.; Kurreck, H.; Möbius, K. *J. Phys. Chem.* **1995**, *99*, 7514. (c) Hasharoni, K.; Levanon, H. *J. Phys. Chem.* **1995**, *99*, 4875. (d) Levanon, H.; Hasharoni, K. *Prog. Reaction Kinetics* **1995**, 20, 1995.

(10) Greenfield, S. R.; Svec, W. A.; Gosztola, D. J.; Wasielewski, M. R. *J. Am. Chem. Soc.* **1996**, *118*, 6767−6777.

(11) The chemical compositions are: E-7 is an eutectic mixture of $R_1C_6H_5$-C_6H_5-CN: $R_1 = C_5H_{11}$ (51%); $R_2 = C_7H_{15}$ (25%); $R_3 = C_8H_{17}O$ (16%); $R_4 = C_5H_{11}C_6H_5$ (8%). The composition of ZLI-4389 is not available.

(12) The soft crystalline is an intermediate phase found in the vicinity of the melting point. It is characterized by some molecular motion of both the solvent and the solute. The transition temperatures of this phase may be estimated from the appearance of TREPR spectra that are the result of solvent-controlled electron transfer. This phase is discussed throughout the text.

(13) Gonen, O.; Levanon, H. *J. Phys. Chem.* **1985**, *89*, 1637.

(14) Regev, A.; Galili, T.; Levanon, H. *J. Chem. Phys.* **1991**, *95*, 7907.

(15) (a) Fajer, P. G.; Bennett, R. L. H.; Polnaszek, C. F.; Fajer, E. A.; Thomas, D. D. *J. Magn. Reson.* **1990**, *88*, 111. (b) Press, W. H.; Flannery, B. P.; Teukolsky, S. A.; Veterling, W. T. *Numerical Recipes. The art of scientific computing*, 1st ed.; Cambridge University Press: Cambridge, 1986.

Table 1. ZFS and Line Shape Parameters for **1** and Its Fragments in LCs

	D[a]	E[a]	A_X:A_Y:A_Z	$\sigma_{\theta'}$ [b]	ϕ_0[b]	σ_ϕ[b]
1	685	34.7	0.85:0.98:1.0	21	52	29
2	714	9.8	0.25:1.0:0.03	23	30	25
5	697	16.9	0.28:1.0:0.08	19	56	27

[a] In 10^{-4} cm^{-1}, uncertainty: 10%. [b] In degree, uncertainty: 10%.

Table 2. Kinetic Parameters of **1** in Toluene and E-7 at Different Temperatures and mw Power

toluene: 5 mW	k_1[a,d]	k_2[a,d]	
170 K	2.3	0.41	
240 K	2.7	2.2	
E-7: 230 K	k_1[b,d]	k_2[b,d]	k_3[b,d]
0.2 mW	2.2	0.34	0.19
100 mW	2.8	1.5	0.14
E-7: 150 K	k'_2[c,d]		k'_3[c,d]
0.2 mW	0.7		0.063
100 mW	1.9		0.062

[a] Fitted with eq 3. [b] Fitted with eq 4. [c] Fitted with eq 12. [d] In 10^6 s^{-1}, uncertainty ±5%.

(Figure 1a), and a narrow 5−7 G width spectrum, at $g \approx 2$, with an *e,a* phase pattern superimposed on the triplet spectrum (Figure 1b,c). The broad spectrum is detectable only in the rigid glass region of toluene i.e., below 177 K, as expected for a triplet EPR spectrum of a π-conjugated system dissolved in traditional glasses (see Tables 1 and 2 for magnetic and kinetic parameters, respectively). The narrow spectrum is detectable throughout a wide temperature range of 100−310 K. Between 177 and 230 K, this spectrum exhibits hyperfine structure (hfs). Below 177 K and above 230 K the narrow spectra become structureless.

The structured spectrum is likely to be due to the radical anion of the naphthalenetetracarboxylic acid diimide (C), where the splittings arise from the 4 naphthyl protons (1.9 G) and from the two nitrogens (0.85 G),[16] as is evident from the simulated spectrum (see also Discussion). Below 177 K, the hfs is unresolved, due to line broadening caused by anisotropic hyperfine interactions, while at temperatures above 230 K the disappearance of the hfs is attributed to electron-electron exchange broadening.

The magnetization time profiles of the narrow signal, $M_y(t)$, are shown in Figure 2a for **1** in toluene at 170 and 240 K. The rise time and decay time of $M_y(t)$ were fit by the exponential expression

$$M_y(t) = -A_1 e^{-t/\tau_1} + A_2 e^{-t/\tau_2} \quad (3)$$

and typical kinetic parameters are given in Table 2. For comparison, the kinetics of $M_y(t)$ in LC are shown in Figure 2b at different microwave (mw) powers and will be discussed below.

A-B-C (1) in LCs. With LCs, additional spectral and dynamic information can be extracted. It should be noted that despite the large difference in the dielectric constants and molecular structure of the different LCs employed, all spectra and kinetics were found to be practically identical.

The TREPR spectra in the **L** || **B** orientation are very similar to that in toluene, exhibiting a triplet spectrum with a 750 G width (Figure 3a). In the **L**⊥ **B** orientation, a ∼1350 G spectral width is observed with an *a,e,e,a,a,e* phase pattern (Figure 3b).

(16) Zhong, C. J.; Kwan, W. S. V.; Miller, L. L. *Chem. Mater.* **1992**, *4*, 1423.

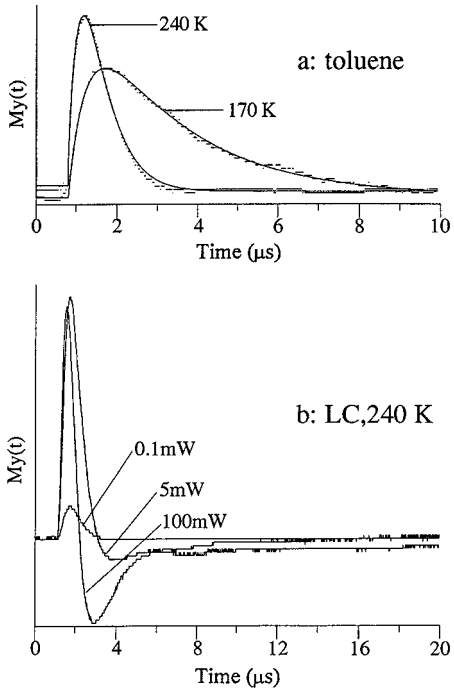

Figure 2. Kinetic traces of the RP (taken at the maximum) in (a) toluene, 5 mW mw power at 170 K and at 240 K. The smooth curves superimposed on the traces are biexponential fits to the data, (b) ZLI-4389 at three different mw power levels at 240 K.

The triplet spectra are observed only in the rigid glass and in the low temperature range of the soft crystalline phases (<240 K).[12] The abrupt disappearance of the triplet spectrum above 240 K is unique, since it has been established by now that triplet EPR spectra in LCs can be observed throughout their fluid nematic phases, i.e., well above room temperature.[8,9] Similar to toluene, a narrow (∼5 G) spectrum with *e,a* polarization pattern is observed at $g \approx 2$, over the entire temperature range of 100−350 K (Figures 3 and 4), with the exception that the hfs are barely observed in the spectra, probably also because of line broadening. Sample orientation in the solid phase (eq 1) affects also the phases of the narrow signal, i.e., *e,a* at **L** || **B** and *a,e* at **L** ⊥ **B** (Figure 3).[17] Such an effect is characteristic to anisotropic interactions and will be discussed below.

The most conspicuous difference between toluene and the LCs used is a phase inversion of the time-evolved narrow spectrum that only occurs in the soft crystalline and nematic phases of the LCs, i.e., *e,a* → *a,e* (Figure 4). No such phenomena is observed in toluene at any temperature. This inversion depends on the mw power as clearly seen in Figure 2b. Moreover, the threshold of phase inversion coincides with the disappearance of the triplet spectrum.

The biphase magnetization curves obtained at high mw powers at the soft crysalline and nematic phase temperatures (Figure 2b) could not be fitted with a single exponential rise and decay as was appropriate for the kinetics in toluene. The following expression was used to fit the data

$$M_y(t) = -A_1 e^{-t/\tau_1} + A_2 e^{-t/\tau_2} - A_3(1 - e^{-t/\tau_2})\cdot e^{-t/\tau_3} \quad (4)$$

This empirical expression describes the situation, where the time profile of $M_y(t)$ accounts for several processes: fast rise (τ_1) followed by a decay, which is made up of two consecutive processes having the same decay times (τ_2), i.e., decay to zero

(17) At high temperatures, in the liquid nematic phase of the LC, the perpendicular orientation is not observed because of the fast alignment of the chromophore to the parallel orientation (see ref 8).

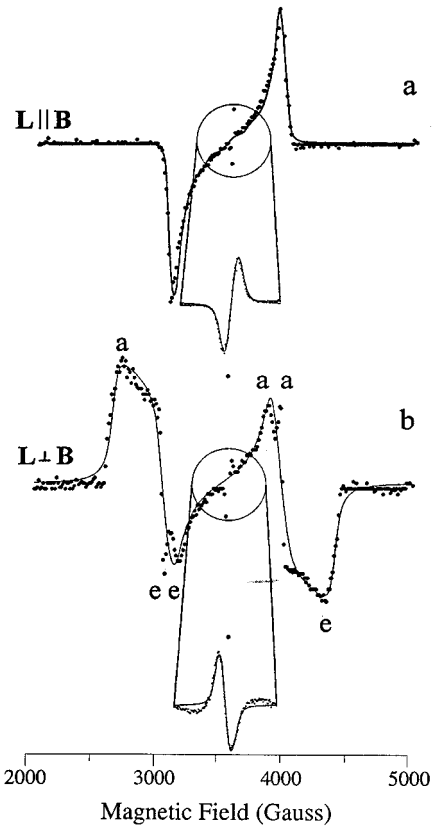

Figure 3. TREPR spectra of the triplet state, A-B-^{3*}C in a LC, 105 mW mw power, 700 ns after the laser pulse (420 nm) at 150 K. The expanded narrow spectra are those of RP signal (scan range is 50 G), observed in the center of the triplet spectra at both orientations: (a) **L** || **B** and (b**) L** ⊥ **B**.

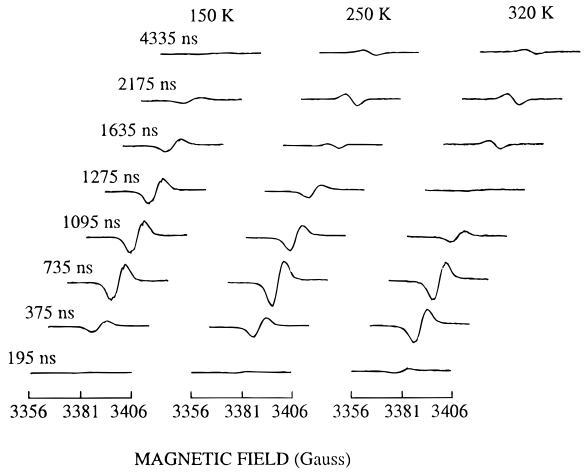

Figure 4. TREPR spectra of $A^{\bullet+}$-B-$C^{\bullet-}$ at three different temperatures in E-7. The spectra at each temperature are presented as a function of the time following the laser pulse (420 nm).

followed by a rise of the inverted signal, and a final slow decay time (τ_3). The physical interpretation of eq 4 will be discussed below.

Control Experiments in LCs. To assist us with the identification of the spectra and elucidation of the excited state reactions, we have carried out control experiments on the separated fragments (Figure 5).

B-C (2). The wide triplet spectrum (Figure 5a) taken at **L** ⊥ **B** (showing all six canonical orientations), exhibits a different polarization pattern than that found for **1**, i.e., *e,e,e,a,a,a* vs *a,e,e,a,a,e*, respectively. All of these transitions are found at the same magnetic field as described above for **1**. In addition,

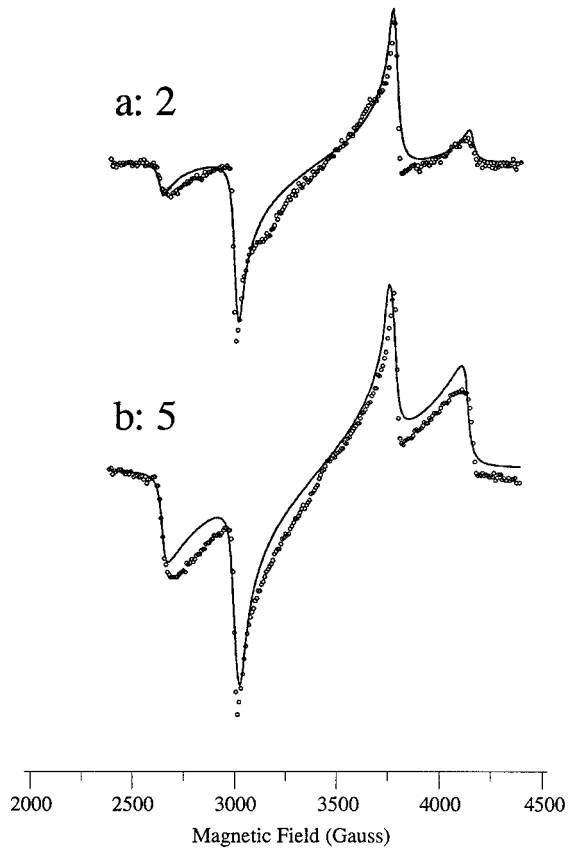

Figure 5. Triplet TREPR spectra of the control compounds **2** (a) and **5** (b) 1300 ns following the laser pulse at 150 K in the **L** ⊥ **B** orientation.

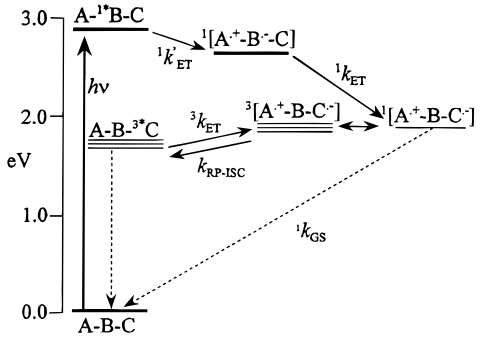

Figure 6. Energy levels diagram of all relevant IET and ISC routes. The energies were determined in toluene (see ref 23).

the narrow $g \approx 2$ signal can also be detected, but with a much smaller S/N than that found in **1**.

B (4) and C (5). Both fragments exhibit only a triplet EPR spectrum, and, also here, the field positions match those of **1**. In fragment **5** the polarization pattern is *e,e,e,a,a,a* at **L**⊥ **B** (Figure 5b). The triplet signal from **4** is very weak, and assignment of the polarization pattern is difficult to elucidate, although it seems to be similar to that of **5**.

To summarize, it is evident that the triplet states in **2**, **4**, and **5** exhibit completely different polarization patterns than that of **1**. On the other hand, the zero-field splitting (ZFS) values in all cases are close since the detected triplet states in these molecules arise from π-systems of comparable dimensions, e.g., the naphthalimide (B) or naphthalenediimide (C).

Discussion

The sequence of IET events is depicted in Figure 6. Selective photoexcitation of the naphthalimide moiety (B) creates the excited singlet state which accepts an electron ($\tau = 8$ ps) from

A to produce the first RP, $A^{\bullet+}$-$B^{\bullet-}$-C.[2] This short-lived RP (430 ps) cannot be detected because of the limited time resolution of TREPR (~100 ns). A subsequent second dark IET (with rate $^1k_{ET}$) creates the second RP, $^1[A^{\bullet+}$-B-$C^{\bullet-}]$ which gives rise to the narrow *e,a* signal (Figures 1b,c and 4). Zeeman and hyperfine induced interactions mix the RP singlet and triplet spin states, i.e., ^{1}RP ↔ ^{3}RP. Thus, concerning $^1[A^{\bullet+}$-B-$C^{\bullet-}]$, apart from recombination to the ground state, an additional decay route involves S-T_0 mixing followed by charge recombination to form the triplet state, A-B-^{3*}C. This triplet state is the origin of the broad spectra (Figures 1a and 3). The following discussion will be divided into two parts, the triplet and the RP spectra, but nevertheless, it should be emphasized that the two species are related to each other.

Triplet Spectra. Although the S/N ratio is poor for the triplet EPR spectrum in toluene, its line shape is similar to that observed in LCs at **L** || **B**, i.e., the two outer (Z) transitions are absent (Figure 1a). This observation is not common as the isotropic distributed triplet spectrum should show all six transitions. Such a spectrum in an isotropic environment could arise only if the molecular tumbling prior to freezing is restricted. Reports of diimide ion π-stacking in solution support this observation.[16,18] If the molecules aggregate to form stacks, which have considerable anisotropic nature, a unidirectionality can be imposed on the alignment of **1** in toluene, such that the spectra are similar to those found in LCs. The line shape analysis of the spectra in toluene could not be carried out using conventional expressions for isotropic matrices.[13,19] Simulations were possible only by using eq 2, which is defined to describe the line shape in LCs, thus confirming the anisotropic nature of the toluene solution, probably caused by π-stacking of the molecules. Supporting evidence for the anisotropic nature of the spectra in toluene is provided by a recent report employing electron-nuclear double resonance spectroscopy of tetraphenylporphyrin photoexcited into its triplet state.[20]

In the LC, the *a,e,e,a,a,e* phase pattern of the **L** ⊥ **B** spectrum indicates unambiguously that the polarization patterns are conserved within a particular triplet EPR transition, i.e., $|^TT_0\rangle$ ↔ $|^TT_{+1}\rangle$ or $|^TT_{-1}\rangle$ ↔ $|^TT_0\rangle$ (the T superscript indicates triplet state eigenfunctions while R indicates RP eigenfunctions). Therefore, triplet formation cannot arise from spin-orbit intersystem crossing (SO-ISC).[21] Such a phase pattern is typical of RP-ISC, and thus an intermediate RP, i.e., $^3[A^{\bullet+}$-B-$C^{\bullet-}]$, is required to realize this polarization pattern.[2] In such a case, the triplet state population via RP-ISC is selective with respect to the high-field levels and not to the molecular zero-field energy levels as in SO-ISC. The nearly equal population ratios (0.8: 0.98:1.0) used to simulate the spectra shown in Figure 3 (Table 1) have no physical meaning in the case of spin-selective SO-ISC, and they reflect the unique case of RP-ISC. The *a,e,e,a,a,e* (Figure 3) pattern can be formed either from overpopulation of $|^TT_0\rangle$ at all orientations, which implies $D > 0$ and S-T_0 mixing in the RP or from overpopulation of $|^TT_{\pm1}\rangle$ at all orientations, implying $D < 0$ and S-$T_{\pm1}$ mixing in the RP. It is possible to differentiate between these two cases from the dependence of the spectral symmetry on the mw power.[22] If $|^TT_0\rangle$ is overpopulated, then at low mw power, both transitions, $|^TT_{-1}\rangle$ ↔ $|^TT_0\rangle$ and $|^TT_0\rangle$ ↔ $|^TT_{+1}\rangle$ will have equal amplitudes. When high mw powers are used, fast $\Delta m_S = \pm2$ relaxation will transfer spin population from one state to the other and signal asymmetry will result. In the other case where the overpopulation is in $|^TT_{\pm1}\rangle$, the $\Delta m_S = \pm2$ relaxation will have no effect on the spectral symmetry.[23] By inspection of the triplet spectra (a typical one is shown in Figure 3) and the kinetic traces (not shown), we find that the high and low field signals are indeed symmetric at low power and become more asymmetric as the mw power is increased. Therefore, we can conclude that $D > 0$ and that S-T_0 is the operative mechanism, which is also feasible for π-orbital spin distribution.

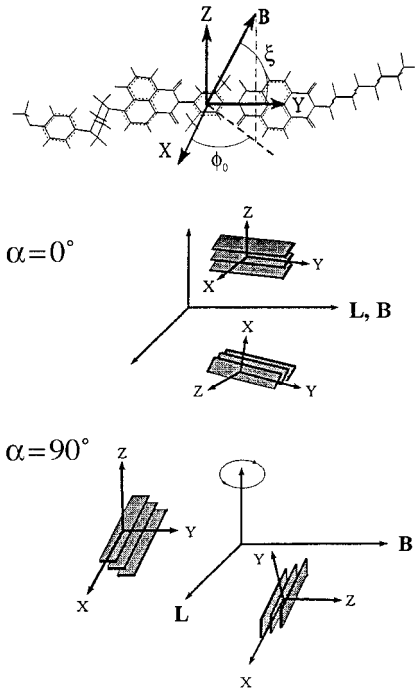

Figure 7. (a) Definition of the relevant angles and molecular axis system superimposed on the minimum energy structure of **1**. (b) Orientation of the π-stacks in the LC with respect to the director and magnetic field at **L** || **B** ($\alpha = 0°$) and at **L** ⊥ **B** ($\alpha = 90°$). The stack size was arbitrarily set to three.

Line shape analysis of the spectra in LCs indicates that **1** does not align parallel to the LC molecules (to the director, **L**) as expected by intuition. This conclusion is based upon the large value (52°) found for ϕ_0, which gives the most probable location of the LC director, **L**, in the molecular plane (Figure 7). This result can be accounted for when the molecular geometry and the π-stacking, mentioned above, are considered. A stack made up of a few molecules with the size of **1** cannot align parallel to **L** because of the LC packing forces. Moreover, the aliphatic, C_8H_{17} tail is found from molecular modeling to be tilted with respect to the A-B-C plane and thus, the perturbation of the stack to the LC molecular alignment becomes more pronounced. Therefore, with the above considerations, the tilted stack alignment depicted in Figure 7b is proposed. It is seen that at **L** || **B**, the out-of-plane axis (*Z*) does not have a component on **B** while in the **L** ⊥ **B** orientation, both *Z* and *X* (or *Y*) can have components on **B**. This implies that as in the well-studied porphyrin triplet spectra in LCs,[14] the stack distribution around **L** is cylindrical.

Unlike the triplet spectra of **1**, the corresponding spectra of the control compounds, **2, 4**, and **5**, exhibit a polarization pattern which is typical of SO-ISC. The population ratios in **2** (Table 1) found from line shape analysis are indicative that SO-ISC is

(18) Miller, L. L.; Zhong, C. J.; Kasai, P. *J. Am. Chem. Soc.* **1993**, *115*, 5982.
(19) Gonen, O.; Levanon, H. *J. Phys. Chem.* **1984**, *88*, 4223.
(20) Kay, C. W. M.; Di valnetin, M.; Möbius, K. *Sol. Energy Mater. Sol. Cells* **1995**, *38*, 111.
(21) Levanon, H.; Norris, J. R. *Chem. Rev.* **1978**, *78*, 185.
(22) Thurnauer, M. C. *Rev. Chem. Intermed.* **1979**, 197.

(23) This test may be carried out provided that the TREPR observation time is faster then $^3T_1$. Indeed, the relaxation times in Table 2 are in the order of 10^{-4}−10^{-5} s which is much longer then the typical TREPR response time (~10^{-7} s).

selective with respect to one of the in-plane zero-field axes of the molecule. A triplet spectrum initiated by RP-ISC does not evolve in **2** because the RP ($B^{\bullet+}$-$C^{\bullet-}$) is formed in low quantities, as is evident from the S/N ratio of the narrow signal. This implies that SO-ISC may also be active in **1** (in low yield) but masked by the strong RP-ISC signal. The LC distribution angles and ZFS parameters (Table 1) are comparable in all molecules which is logical when the similar structure is considered. The small value of E is consistent with an axial symmetry of all four molecules. From the point dipole approximation

$$D \approx \frac{3}{4}\frac{(g\beta)^2}{r^3} \tag{5}$$

we calculate a value of ~3.30 and ~3.27 Å for the spin−spin separation in **1** and **2**, respectively. This indicates that the triplet is localized on a small fragment of the molecules, probably on the naphthalene moiety. From measurements of the phosphorescence spectra in methyltetrahydrofuran at 77 K, this triplet state is found to be localized on the naphthalenediimide (C).[24] The ZFS parameters of these molecules are smaller then those reported for naphthalene in a nematic LC.[25] This difference indicates that the electrons are delocalized to some extent beyond the naphthalene ring in the naphthalenediimide.

RP Spectra. The most noticeable difference between the RP spectra in LCs and those in toluene is the large, three orders of magnitude greater amplitude of the LC spectra. The unusual signal intensities are probably due to the combined effects of the high degree of spin polarization and sample orientation by the LC. This is most conspicuous in the 240−250 K range, which is in the soft crystalline region, just below the crystalline-nematic phase transition (eq 1), where only restricted molecular motion is allowed.

The mixed phase pattern (*e*,*a*) of the RP spectra is indicative that it is spin polarized. Such polarization in a system, where the electron donors and acceptors are held together in a fixed distance develops, in distinguishable time steps, various IET processes within the molecule (Figure 6).[26,27] If an IET takes place in one step, the only polarization mechanism which can be operative is the correlated RP mechanism (CRPM), where the two electron spins are interacting during the time of TREPR observation.[28,29] When the IET scheme becomes a multistep process, then polarization may also evolve via the radical pair mechanism (RPM), provided that the magnetic coupling between the radicals is insignificant at the time of TREPR observation.[27] Due to the short lifetime (430 ps in toluene at room temperature[2]) of the first intermediate RP ($A^{\bullet+}$-$B^{\bullet-}$-C), magnetic interactions cannot build up and thus, CRPM is the most probable mechanism for spin polarization in the second RP, which is detected, i.e., $A^{\bullet+}$-B-$C^{\bullet-}$. The EPR transitions in the RP at low temperatures are depicted in Figure 8a. Following S-T_0 mixing, the pure singlet and T_0 states are no longer eigenfunctions of the system because $|^{R}T_0\rangle$ has some singlet character $|\psi_a\rangle = (T_0 + \lambda S)$ and $|S\rangle$ has some triplet character

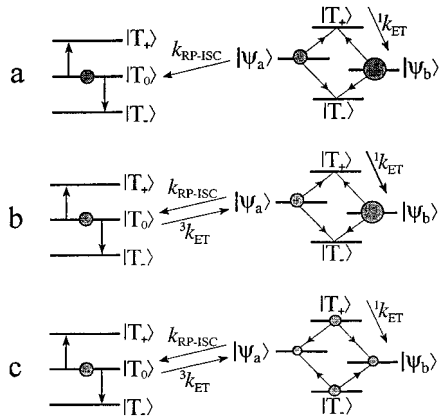

Figure 8. Schematic EPR transtions diagram for the triplet (left) and RP (right) states, the shadowed circles indicate spin population: (a) low temperature case where the back IET is not active; (b) high temperature, low mw power; and (c) high temperature, high mw power.

$|\psi_b\rangle = (S + \lambda T_0)$. The states labeled as $|\psi_{a,b}\rangle$, are to distinguish them from the pure singlet and triplet states. EPR transitions between all four spin levels become allowed, and, as shown previously,[27,30,31] they will have the same amplitude since the signal intensity is the product of the population difference with the transition probability. Specifically, the $|\psi_a\rangle \leftrightarrow |T_+\rangle$ transition is the product of a small population difference with a large transition probability, while the $|\psi_b\rangle \leftrightarrow |T_-\rangle$ is the product of a large population difference with a small transition probability. It is noteworthy, that equal amplitudes of the correlated pair transitions are expected only in the absence of chemical reactions from $|\psi_{a,b}\rangle$ and/or relatively slow spin relaxation time.

With these reasonable asuumptions, the CRPM spectra were simulated using conventional expressions for the position (ω_{ij}) and intensity (I_{ij}) of the EPR transitions,[31,32] i.e.

$$\begin{aligned} \omega_{12} &= \omega_0 - \Omega - J + D_{zz} \\ \omega_{34} &= \omega_0 - \Omega + J - D_{zz} \\ \omega_{13} &= \omega_0 + \Omega - J + D_{zz} \\ \omega_{24} &= \omega_0 + \Omega + J - D_{zz} \end{aligned} \tag{6}$$

and

$$I_{12} = I_{13} = -I_{24} = -I_{34} = Q_2/8\Omega^2 \tag{7}$$

where ω_0 is the center of resonance

$$\omega_0 = \frac{1}{2}(g_1 + g_2)\mu_B\hbar^{-1}\mathbf{B_0} + \frac{1}{2}(\sum_i a_{1i}m_{1i} + \sum_j a_{2j}m_{2j}) \tag{8}$$

and $\Omega^2 = (J + D_{zz}/2)^2 + Q^2$. The mixing term between singlet and triplet states is

(24) Determined by measuring the out-of-phase emission using a fluorimeter (PTI) with the excitation light chopped at 200 Hz.

(25) (a) Krebs, P.; Sackmann, E.; Schwarz, J. *Chem. Phys. Lett.* **1971**, *8*, 417. (b) Sackmann, E. In *Applications of Liquid Crystals*; Meier, G., Sackmann, E., Grabmaier, J. G., Eds.; Springer-Verlag: Berlin, 1975; pp 21−81.

(26) Pedersen, J. B. *FEBS Lett.* **1979**, *97*, 305.

(27) Norris, J. R.; Morris, A. L.; Thurnauer, M. C.; Tang, J. *J. Chem. Phys.* **1990**, *92*, 4239.

(28) Hore, P. J.; Hunter, D. A.; McKie, C. D.; Hoff, A. J. *Chem. Phys. Lett.* **1987**, *137*, 495.

(29) Closs, G. L.; Forbes, M. D. E.; Norris, J. R. *J. Phys. Chem.* **1987**, *91*, 3592.

(30) Morris, A. L.; Norris, J. R.; Thurnauer, M. C. In *Biophysics*; Michel-Beyerle, M. E., Ed.; Springer-Verlag: Berlin, 1990; Vol. 6, pp 423−434.

(31) Hore, P. J. In *Advanced EPR. Applications in biology and biochemistry*; Hoff, A. J., Ed.; Elsevier: Amsterdam, 1989; pp 405−440.

(32) Stehlik, D.; Bock, C. H.; Petersen, J. *J. Phys. Chem.* **1989**, *93*, 1612.

$$Q = \frac{1}{2}(g_1 - g_2)\mu_B\hbar^{-1}\mathbf{B_0} + \frac{1}{2}(\sum_i a_{1i}m_{1i} - \sum_j a_{2j}m_{2j}) \quad (9)$$

$g_{1,2}$ are the g-factors of radicals 1 and 2, a_{1i} and a_{2j} are the hyperfine constants of radicals 1 and 2, J is the exchange integral, and

$$D_{zz} = D(3\cos^2\xi - 1) \quad (10)$$

where D is the dipolar interaction strength and ξ is the angle between the dipolar axis and the magnetic field direction (see also Figure 7a).

Simulation of the CRPM spectrum does not require knowledge of the charge separated radicals ($A^{\bullet+}$-B-$C^{\bullet-}$) g-factors but only of their difference, which was one of the varied parameters in the fit and found to be $\sim 3 \times 10^{-4}$. In the simulations, J was assumed to be zero because of its exponential dependence on the spin-spin separation.[33] The value of D (−2.6 G), found by the line shape analysis, corresponds to a separation of ∼21 Å between the two electron spins, which agrees with the center-to-center separation between A and C (24 Å), as found from molecular modeling. The negative sign of D is expected for an axial RP (head-to-tail).[21] The large value (65°) of the dipolar angle, ξ, is consistent with the results from the triplet line shape analysis which found large values for ϕ_0. This result indicates that the molecular plane is tilted with respect to the magnetic field, probably also because of molecular π-stacking. The dipolar angle, ξ, can also be estimated from the CRPM sign rule, with the assumption that $J = 0$[31]

$$\Gamma = -\mu\cdot\mathrm{sign(D)}\cdot\mathrm{sign}(3\cos^2\xi - 1) = \begin{cases} -\mathrm{EA} \\ +\mathrm{AE} \end{cases} \quad (11)$$

where μ is −1 or +1 for a singlet or triplet precursor, respectively. To meet with $D < 0$ and a singlet precursor, the dipolar angle must be $\xi \leq 54°$, which is lower by 16% than that obtained by the line shape simulation. This apparent discrepancy is probably due to the assumptions made on J and the expected errors in the line shape simulations. Nevertheless, the results are fully consistent with the unique orientation of the molecular assembly in the LC.

The phase inversion of the RP spectrum upon sample rotation in the solid phase of the LC,[17] e.g., *e,a* ($\mathbf{L} \parallel \mathbf{B}$) → *a,e* ($\mathbf{L} \perp \mathbf{B}$) is evident from eq 10 when the dipolar angle is replaced by $\xi + \alpha$ (where α is the sample rotation angle, Figure 7b). The different peak-to-peak width expected for the two sample orientation is absent here (note the comparable width of the expanded spectra in Figure 3) because inhomogeneous hyperfine broadening is the dominant feature of the line shape, thus, masking the smaller dipolar contribution to the line width.

The *e,a* → *a,e* phase change of the RP spectrum (Figure 4), that occurs only in LCs in the fluid phases, originates from repopulation of the RP from the triplet state (Figure 6). This is based on the following arguments. The triplet state of **1** (A-B-^{3*}C) can decay by two routes. The first involves deactivation to the ground state and the second is via a thermal IET step to reform ^{3}[$A^{\bullet+}$-B-$C^{\bullet-}$]. The opposite sign of the RP spectra at long times (∼1 μs) following the laser pulse (Figure 4) indicates that the precursor for this RP is a triplet state, i.e., A-B-^{3*}C, implying that μ in eq 11 is positive. The disappearance of the triplet spectra above 240 K concurrently with the appearance of the phase change at the same temperature is not accidental. At these elevated temperatures, back IET, A-B-^{3*}C → ^{3}[$A^{\bullet+}$-B-$C^{\bullet-}$], is dominant, while the decay of the triplet to the ground state is the main decay route below 240 K.

(33) $J(r)$ is approximated by the phenomenoligical expression: $J(r) = J_0e^{-\lambda r}$, where J_0 and λ are constants: Molin, Yu. N.; Salikhov, K. M.; Zamaraev, K. M. *Spin Exchange, Principles and Applications in Chemistry and Biology*, Springer-Verlag: Heidelberg, 1980; pp 34−35. Although the exact mechanism dictating the rate of fall off is not yet fully understood, based on the experimental data, the assumption that $J = 0$ for a spin−spin separation of 24 Å is reasonable and meets with previous studies (ref 9, above).

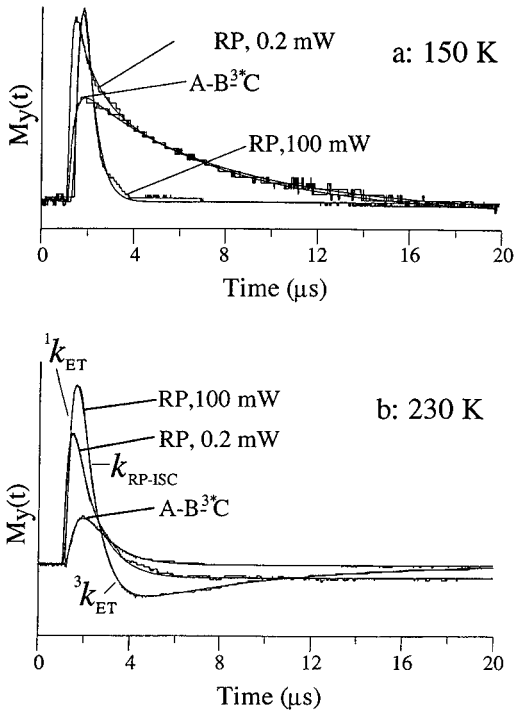

Figure 9. Kinetic traces of the RP and triplet (A-B-^{3*}C) in E-7 at high and low mw power levels: (a) 150 K, the components of the RP decay curve are indicated, and (b) 230 K, the components of the RP rise and decay are given in terms of Figure 6. The smooth curves superimposed on the traces are best fits to the data using eq 4.

The absence of these phenomena in toluene and in LCs at low temperatures is consistent with our previous studies describing the unique effect that LCs have on solvent controlled IET.[9] Contrary to the forward IET ($^1k_{ET}$ in Figure 6) which shows no solvent- and a weak temperature-dependence, the back IET ($^3k_{ET}$) falls into the class of solvent-controlled IET processes. Such IET reactions in LCs are affected by the existence of a potential barrier to solvent-dipole reorientation.[9] It causes the solvent reorientation, which governs the adiabatic IET rate, to behave similarly to the LC order parameter, which in the fluid nematic phase exhibits a slow change with temperature. Based on such a correlation, the back IET product can be observed throughout the 220−350 K range which corresponds to the soft crystalline and fluid nematic phases of the LCs (eq 1).

To explain the difference between the RP kinetics and signal behavior at low and high temperatures shown in Figure 4, we present in Figure 9 the kinetics of both the RP and the triplet (A-B-^{3*}C) for two cases.

(a) At low temperatures (e.g., 150 K) and low mw power, the RP rise time was found to be temperature independent with a rate in the order of 2.5×10^6 s^{-1}. Its magnetization was fitted with a biexponential decay kinetics according to

$$M_y(t) = B_2e^{-t/\tau'_2} + B_3e^{-t/\tau'_3} \quad (12)$$

This decay of the RP (Figure 9a) shows a fast component (τ'_2) and a slower one (τ'_3). As the mw power is increased, the RP decay becomes monoexponential characterized by τ'_2. For clarity, we also show the triplet kinetics, i.e., the formation of

(A-B-^{3*}C) signal. It is clear that the monoexponential decay of this triplet is identical with the slow component of the RP magnetization, τ'_3, at low mw power. The RP fast decay time, τ'_2, is associated with the formation of (A-B-^{3*}C), which corresponds to the RP decay rate, k_{RP-ISC} (the rate constants are given in Table 2).

The biexponential decay of the RP is indicative of two simultaneous decay routes: (1) ^{3}[A$^{\bullet+}$-B-C$^{\bullet-}$] → A-B-^{3*}C → A-B-C and (2) ^{1}[A$^{\bullet+}$-B-C$^{\bullet-}$] → A-B-C (Figure 6). At low mw power, route 1 is preferred because $|\psi_{a,b}\rangle$ is overpopulated, and, as suggested above, it is the source for populating A-B-^{3*}C (Figure 8a); this route is dominated by (τ'_3). Therefore, the slow decay component of the RP arises from formation of the triplet via RP-ISC and decay to the ground state through SO-ISC, i.e., the detected signal (slow component) is that of A-B-^{3*}C. Under these experimental conditions, route 2 is less favorable, and the ratio between the two decay components, $B_2(\tau'_2)/B_3(\tau'_3)$ is approximately equal to 0.1. At high mw power, route 2 is preferred since $|\psi_{a,b}\rangle$ are depleted by EPR induced enhanced population transfer, $|\psi_{a,b}\rangle \leftrightarrow |^RT_{\pm1}\rangle$, thus decreasing the yield of A-B-^{3*}C formation. Such a behavior was indeed predicted for RPs at high mw fields.[34] Route 2 is dominated by (τ'_2), and in this case the ratio between the two decay components, $B_2(\tau'_2)/B_3(\tau'_3)$, is about 20. Since τ'_2 (0.2 mW) > τ'_2 (100 mW), it may be assumed that at low mw power the fast component is the sum of decay via route 2 and the formation of A-B-^{3*}C.

(b) At high temperatures (e.g., >220 K), where RP phase inversion occurs (Figures 4 and 9b), the above description is no longer complete since the additional route of back IET ($^3k_{ET}$) becomes active and should be taken into account. Kinetic parameters in this case were obtained by fitting eq 4 to the experimental results (Figure 9b). Phase inversion strongly depends on the mw power, becoming more pronounced upon increasing the temperature and mw power. The comparable magnitude of the triplet rise (1.3×10^6 s^{-1}) and k_2 (Table 2) indicates that the RP decays with a rate, k_{RP-ISC}, similar to the rate $^3k_{ET}$ to form the RP from A-B-^{3*}C.

As shown in Figure 8b, at low mw power, the back IET repopulates $|\psi_{a,b}\rangle$, and the EPR transitions are the same as described above, for the low temperature case, thus the slow decay at 150 K (τ'_3 above) is not detected here. Under high mw fields (Figure 8c), spin population is transferred from $|\psi_{a,b}\rangle$ to $|^RT_{\pm1}\rangle$ resulting in an inversion of the EPR signal, as indeed shown by the kinetic traces shown in Figure 9b. Again, such a behavior was predicted earlier.[34]

Supporting evidence for the ^{3}RP repopulation route is provided by the relationship between the A-B-^{3*}C and RP kinetics (Figure 9b). It can be noticed that the triplet magnetization decay curve approaches zero intensity at the same time where the inverted RP signal reaches a maximum (negative phase). Similar correlation between decay of a triplet state and rise of a RP signal was observed in porphyrin-quinone molecules, and, as in the present case, it was interpreted as triplet initiated IET.[9,35]

We have shown that a rod-like electron donor−acceptor triad exhibits electron transfer rates and spin dynamics that are strongly influenced by the anisotropic solvation properties of nematic LCs. In this medium the spin dynamics of both the radical pair and the corresponding molecular triplet state formed upon radical pair recombination are strongly analogous to those observed exclusively in the photosynthetic reaction-center proteins. The LC medium allows us to modify both the rates and energetics of the charge separation and recombination processes, controlled by the microenvironment in the vicinity of the donor−acceptor triad. The use of LCs for electron transfer studies potentially can provide us with insights into the role of ordered media, such as proteins, in controlling electron transfer reaction rates.

Acknowledgment. We are grateful to Dr. A. Berg and Mrs. T. Galili for helpful discussions. This work was partially supported by a U.S.-Israel BSF grant (H.L.), by the Deutsche Forschungsgemeinschaft (H.L.), by a Volkswagen grant (H.L.), and by the Division of Chemical Sciences, Office of Basic Energy Science, U.S. Department of Energy under contract W-31-109-ENG-38 (M.R.W.). S.R.G. is supported by a Distinguished Postdoctoral Fellowship from the U.S. Department of Energy. A special grant of the Erna and Victor Hasselblad Foundation (H.L.) is highly acknowledged. The Farkas Research Center is supported by the Minerva Gesellschaft für die Forschung, GmbH, München, FRG. This work is in partial fulfillment of the requirements for a Ph.D. degree (K.H.) at the Hebrew University of Jerusalem.

JA961919E

(34) Salikhov, K. M.; Molin, Y. N. *J. Phys. Chem.* **1993**, *97*, 13259.

(35) Lendzian, F.; von Maltzan, B. *Chem. Phys. Lett.* **1991**, *180*, 191.